A high-salt diet promotes hypertrophic scarring through TRPC3-mediated mitochondrial Ca^{2+} homeostasis dysfunction

Weijie Xia [a], Qianran Wang [b], Shaoyang Lin [b], Yuanyuan Wang [a], Junbo Zhang [a], Hailin Wang [a], Xia Yang [c], Yingru Hu [b], Huaping Liang [c], Yuangang Lu [a], Zhiming Zhu [b], Daoyan Liu [b,c,*]

[a] Department of Plastic & Cosmetic Surgery, Research Institute of Surgery, Daping Hospital, Army Medical University, Chongqing 400042, PR China
[b] Department of Hypertension and Endocrinology, Center for Hypertension and Metabolic Diseases, Daping Hospital, Army Medical University (Third Military Medical University), Chongqing 400042, PR China
[c] Department of Wound Infection and Drug, State Key Laboratory of Trauma, Burn and Combined Injury, Daping Hospital, Army Medical University (Third Military Medical University), Chongqing 400042, PR China

ABSTRACT

Diet High in salt content have been associated with cardiovascular disease and chronic inflammation. We recently demonstrated that transient receptor potential canonical 3 (TRPC3) channels regulate myofibroblast transdifferentiation in hypertrophic scars. Here, we examined how high salt activation of TRPC3 participates in hypertrophic scarring during wound healing. In vitro, we confirmed that high salt increased the TRPC3 protein expression and the marker of myofibroblast alpha smooth muscle actin (α-SMA) in wild-type mice (WT) primary cultured dermal fibroblasts but not $Trpc3^{-/-}$ mice. Activation of TRPC3 by high salt elevated cytosolic Ca^{2+} influx and mitochondrial Ca^{2+} uptake in dermal fibroblasts in a TRPC3-dependent manner. High salt activation of TRPC3 enhanced mitochondrial respiratory dysfunction and excessive ROS production by inhibiting pyruvate dehydrogenase action, that activated ROS-triggered Ca^{2+} influx and the Rho kinase/MLC pathway in WT mice but not $Trpc3^{-/-}$ mice. In vivo, a persistent high-salt diet promoted myofibroblast transdifferentiation and collagen deposition in a TRPC3-dependent manner. Therefore, this study demonstrates that high salt enhances myofibroblast transdifferentiation and promotes hypertrophic scar formation through enhanced mitochondrial Ca^{2+} homeostasis, which activates the ROS-mediated pMLC/pMYPT1 pathway. TRPC3 deficiency antagonizes high salt diet-induced hypertrophic scarring. TRPC3 may be a novel target for hypertrophic scarring during wound healing.

1. Introduction

A high salt (NaCl) diet has been implicated in cardiac hypertrophy, chronic inflammation and noninflammatory innate immune cell activation [1–3]. More than 50% of people globally are salt-sensitive, and high salt intake is a significant etiological factor [4]. Long-term high salt intake sodium ions accumulate within the skin independent of the kidney [5,6]. Hypertrophic scar formation by

* Corresponding author. Department of Hypertension and Endocrinology, Center for Hypertension and Metabolic Diseases, Daping Hospital, Army Medical University (Third Military Medical University), Chongqing 400042, PR China.
E-mail address: liudaoyan@tmmu.edu.cn (D. Liu).

collagen-1 (Col1a1) and fibronectin mediates extracellular matrix (ECM) remodeling, and α-smooth muscle actin (α-SMA)-expressing myofibroblasts play central roles [7,8]. Extracellular environment alterations and ECM tension-activating myofibroblasts considerably influence the degree of scarring [9,10]. Cellular sensors such as Ca^{2+} channels and actin filaments are associated with wound scarring [11,12]. Many studies have shown that the contractility of fibroblasts is positively correlated with the level of a-SMA expression [13, 14]. However, it remains unknown whether a high salt diet regulates myofibroblast differentiation associated with hypertrophic scar formation during wound healing.

Transient receptor potential channel canonical 3 (TRPC3) is a mitochondrial membrane component that influences the uptake of calcium and generation of reactive oxygen species (ROS). We have recently shown that TRPC3 activation could result in the release of elevated endoplasmic reticulum (ER) Ca^{2+} reserves and mitochondrial Ca^{2+} uptake in VSMCs [15]. Fibroblasts, as nonexcitable cells, are mainly regulated by store-operated calcium entry for intracellular Ca^{2+} signaling [16]. Recent studies revealed that Ca^{2+}-binding proteins were elevated in fibroblasts related to scarring in burn-wounded skins [17]. Activation of Ca^{2+} occurred in fibroblasts originating from hypertrophic scars but not in keloid-originating fibroblasts [18]. Our recent study demonstrated that increased TRPC3-mediated Ca^{2+} signaling regulated myofibroblast differentiation in hypertrophic scars of dermal skin [19]. TRPC3 is a salt-sensitive ion channel. The mechanism of how high salt activation of TRPC3 participates in hypertrophic scarring during wound
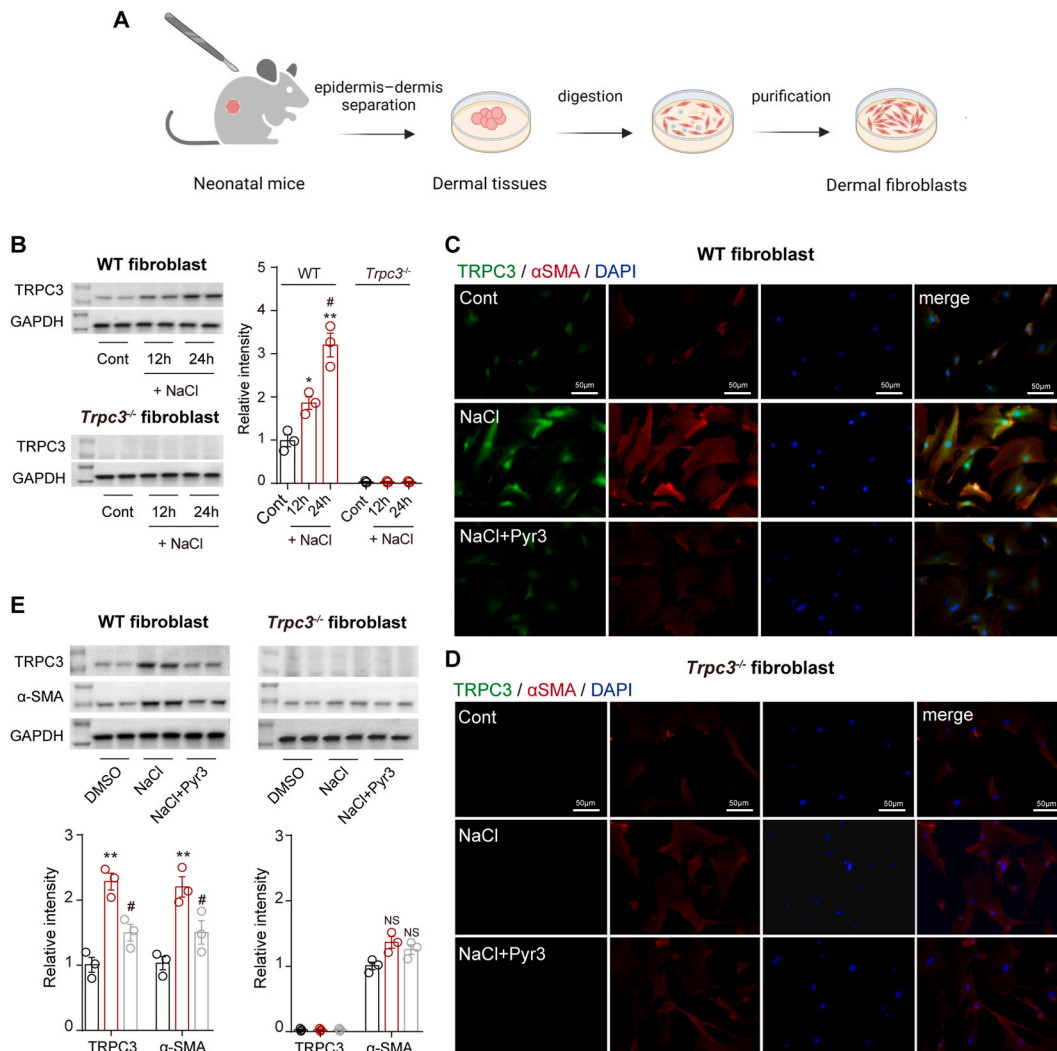

Fig. 1. Effect of high NaCl on TRPC3 and the myofibroblast marker α-SMA in cultured dermal fibroblasts. (A) Schematic representation of primary dermal fibroblast culture protocols. **(B)** Western blot analysis of TRPC3 protein expression in dermal fibroblasts under treatment with NaCl (20 mmol/L, 12 h and 24 h) or control conditions without NaCl treatment (Cont) from WT mice and *Trpc3*$^{-/-}$ mice. **$P < 0.01$, ***$P < 0.001$ vs. control (Cont). Two-tailed Mann–Whitney test. **(C and D)** Immunofluorescence staining of myofibroblast differentiation and αSMA$^+$ (red), TRPC3 (green) and nucleic acid staining (blue) in dermal fibroblasts from WT mice or *Trpc3*$^{-/-}$ mice. **(E)** Western blot analysis of α-SMA and TRPC3 expression was quantified over the control in dermal fibroblasts from WT mice or *Trpc3*$^{-/-}$ mice. **$P < 0.01$ vs. control (Cont). $^{\#}P < 0.05$ vs. NaCl group (NaCl). NS, no significant difference. Unpaired 2-tailed *t*-test. Data are the mean ± SEM, n = 3. (For interpretation of the references to colour in this figure legend, the reader is referred to the Web version of this article.)

healing is still unknown.

Mitochondrial Ca^{2+} homeostasis is the basis for the regulation of mitochondrial ROS production [20,21]. Furthermore, in fibroblasts and keratinocytes, myosin light chain (MLC) and myosin phosphatase target subunit 1 (MYPT1) are key mediators of cell proliferation, survival, and motility [22,23]. In vascular smooth muscle, Rho kinase (ROCK) activates the myosin binding subunit of MLC phosphatase of phosphorylation, leading to elevation in myosin phosphorylation as well as contraction [24]. We previously reported that TRPC3-mediated mitochondrial Ca^{2+} uptake regulated myofibroblast transdifferentiation in dermal fibroblasts involved in hypertrophic scars [19]. However, it is unknown whether high salt intake through TRPC3-mediated calcium disturbance promotes hypertrophic scar formation during wound healing. We aimed to elucidate the mechanism of TRPC3 activation by high salt in hypertrophic scars. TRPC3 may represent a novel prevention target for hypertrophic scars in wound healing.

2. Results

2.1. High NaCl increases TRPC3 and the myofibroblast marker αSMA in primary dermal fibroblasts

First, we examined the effect of high NaCl on TRPC3 protein expression in primary cultured dermal fibroblasts from WT and
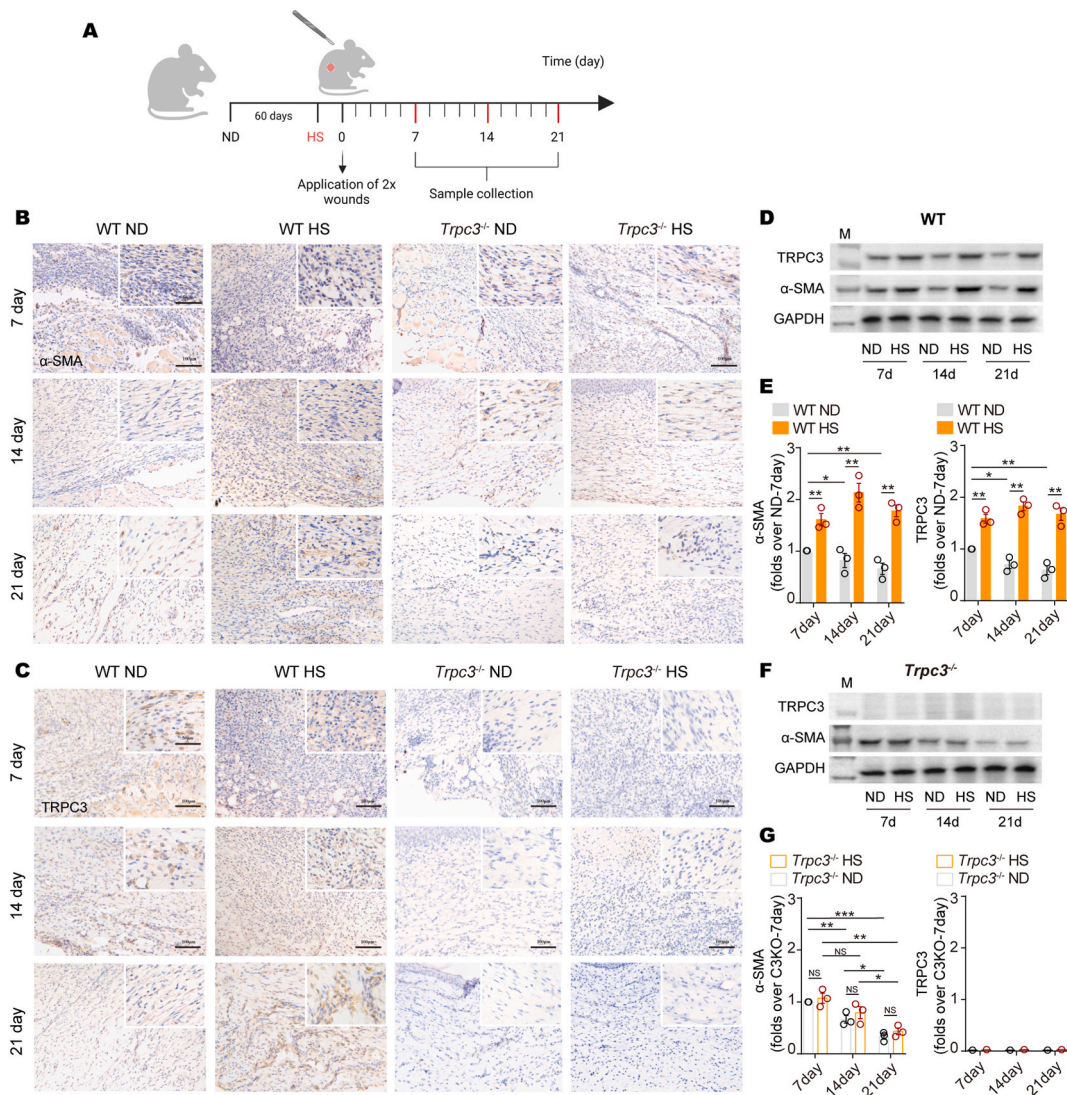

Fig. 2. Effect of high salt on TRPC3 promotes myofibroblast differentiation in vivo. (**A**) WT mice or $Trpc3^{-/-}$ mice were fed a normal diet (0.25% NaCl, ND) or an 8% high salt diet (HS) for 2 months, and then two cutaneous wounds were applied to the backs of mice that were fed an ND or HS for 21 days. (**B**) Immunohistochemical staining of TRPC3 and α-SMA in wound tissue sections after injury (7, 14, 21 days). The right-up panel is high magnification. Scale bars: 50 and 100 μm. (**D-G**) Quantification of TRPC3 and α-SMA protein expression in wound tissue sections after injury (7, 14, 21 days). *$P < 0.05$, **$P < 0.01$, ***$P < 0.001$. NS, no significant difference. Unpaired 2-tailed t-test. Data are the mean ± SEM, n = 3.

$Trpc3^{-/-}$ mice. Western blotting confirmed that high NaCl treatment significantly increased TRPC3 protein expression in primary dermal fibroblasts of WT but not $Trpc3^{-/-}$ mice (Fig. 1A–B). Moreover, high NaCl treatment significantly elevated myofibroblast differentiation by increasing the protein expression of the myofibroblast marker α-SMA. These effects could be inhibited by the TRPC3 inhibitor Pyr3 in primary dermal fibroblasts from WT but not $Trpc3^{-/-}$ mice (Fig. 1C–D). In addition, high NaCl treatment significantly elevated the protein expression of TRPC3, α-SMA, Col1a1 and fibronectin in cultured primary dermal fibroblasts from WT mice but not $Trpc3^{-/-}$ mice, and the effect of high NaCl could be inhibited by Pyr3 (Fig. 1E, Supplemental Figs. 1A–1B). In order to excluded the influence of osmotic pressure increase caused by high salt treatment. We used mannitol as control group. Quantitative real-time PCR (RT−PCR) demonstrated that only high concentrations of NaCl but not mannitol significantly elevated the mRNA levels of TRPC3 and α-SMA in cultured primary dermal fibroblasts from WT but not $Trpc3^{-/-}$ mice (Supplemental Figs. 1C–1D). A high concentration of NaCl did not reduce dermal fibroblast viability (data not shown). Altogether, these results indicate that high NaCl concentrations upregulate TRPC3 and α-SMA expression in dermal fibroblasts in a TRPC3-dependent manner.

2.2. A high salt diet promotes myofibroblast differentiation and exaggerated wound fibrosis in vivo

Next, we further investigated the effect of a long-term high salt diet on myofibroblast differentiation and collagen deposition in vivo. Two wounds 8 mm in diameter were created on the backs of the mice (Fig. 2A). The protein expression of TRPC3 and α-SMA showed significant enhancement in wound granulation tissues of WT mice fed an HS compared to ND. More importantly, these effects
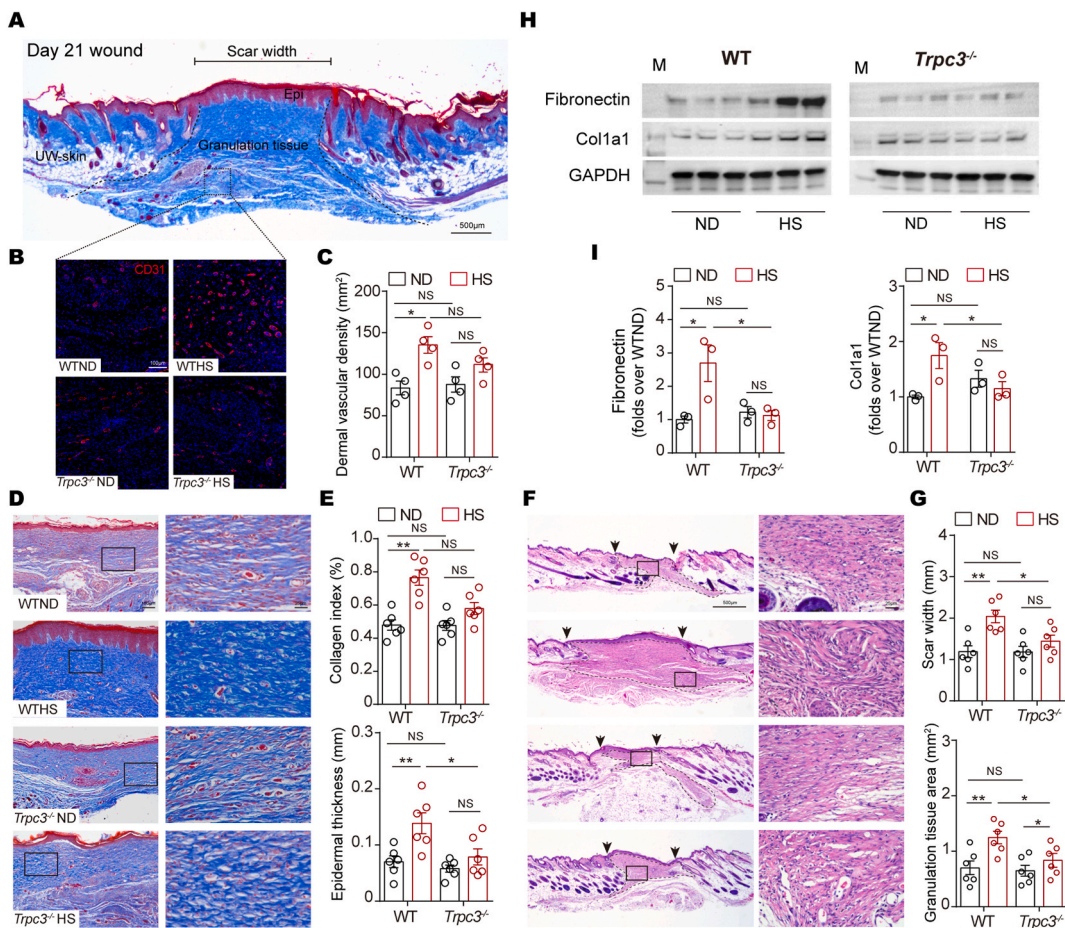

Fig. 3. High salt promotes skin wound fibrosis in a TRPC3-dependent manner. (A) Schematic indicating the measurements derived from histology at 21 days after injury. The dotted line indicates the border between the unwounded skin and granulation tissue. Scale bars: 500 μm. (B and C) Immunofluorescence staining and analysis of CD31 (revascularization) in wound tissue sections at 21 days after injury. Scale bars: 100 μm (D and E) Trichrome staining of the collagen index (%) and epidermal thickness in the wound bed at 21 days after injury. The right panel is high magnification of the black boxes in the left panel. Scale bars: 100 and 25 μm. (F and G) H&E staining of WT and $Trpc3^{-/-}$ mouse wounds used for analysis of scar width and granulation tissue area at 21 days after injury. The right panel is high magnification of the black boxes in the left panel; black dotted lines, the wound granulation tissue areas; black arrows, original wound edges. Scale bars: 500 and 25 μm. (H and I) Quantitative data of fibronectin and Col1a1 protein were analyzed. *$P < 0.05$, *$P < 0.01$ vs. their ND. n = 3.*$P < 0.05$, **$P < 0.01$. NS, no significant difference. Unpaired 2-tailed t-test. Data are the mean ± SEM.

were absent in *Trpc3*$^{-/-}$ mice (Fig. 2B–G). Furthermore, we tested dermal myofibroblast differentiation by immunofluorescence staining in vivo. The results showed that a chronic high salt diet significantly increased α-SMA$^+$ and TRPC3$^+$ cell in wounded skin tissues of WT mice fed an HS compared to ND. However, this effect was not detected in *Trpc3*$^{-/-}$ mice fed an HS diet (Supplemental Figs. 2A–C). To analyze the effect of high salt intervention on skin fibrosis, we collected skin wounds for morphological examination at 21 days after injury (Fig. 3A). Masson and HE staining analysis revealed that a high salt concentration diet significantly increased the collagen index, epidermis thickness, scar width and granulation tissue area (Fig. 3D–G). However, *Trpc3*$^{-/-}$ mice significantly attenuated these effects of high salt. In particular, the wound bed in WT mice on an HS showed disorganized and misaligned arrangement in collagen fibers and clusters of fibroblasts and myofibroblasts, which represent active fibroproliferative reactions at 21 days after injury (Fig. 3D and F). Meanwhile, the vascular density was significantly elevated in the granulation tissue from WT mice fed an HS compared to ND (Fig. 3B–C), and protein expression of Col1a1 and fibronectin in granulation tissues also showed a similar trend at 21 days after injury (Fig. 3H–I). Meanwhile, we detected the coexpression of the fibroblast marker Vimentin and the myofibroblast marker α-SMA in wound skin tissues at 7 days after injury, and the data indicated that the coexpression of Vimentin and α-SMA proteins was significantly elevated at the wound edges from WT mice fed an HS compared to ND. However, TRPC3 deficiency significantly attenuated these effects of high salt (Supplemental Figs. 3A–3B). These findings indicate that a long-term high salt diet enhances fibroblast differentiation into myofibroblasts, leading to hypertrophic scar formation during wound healing. TRPC3 deficiency may attenuate this effect of high salt.
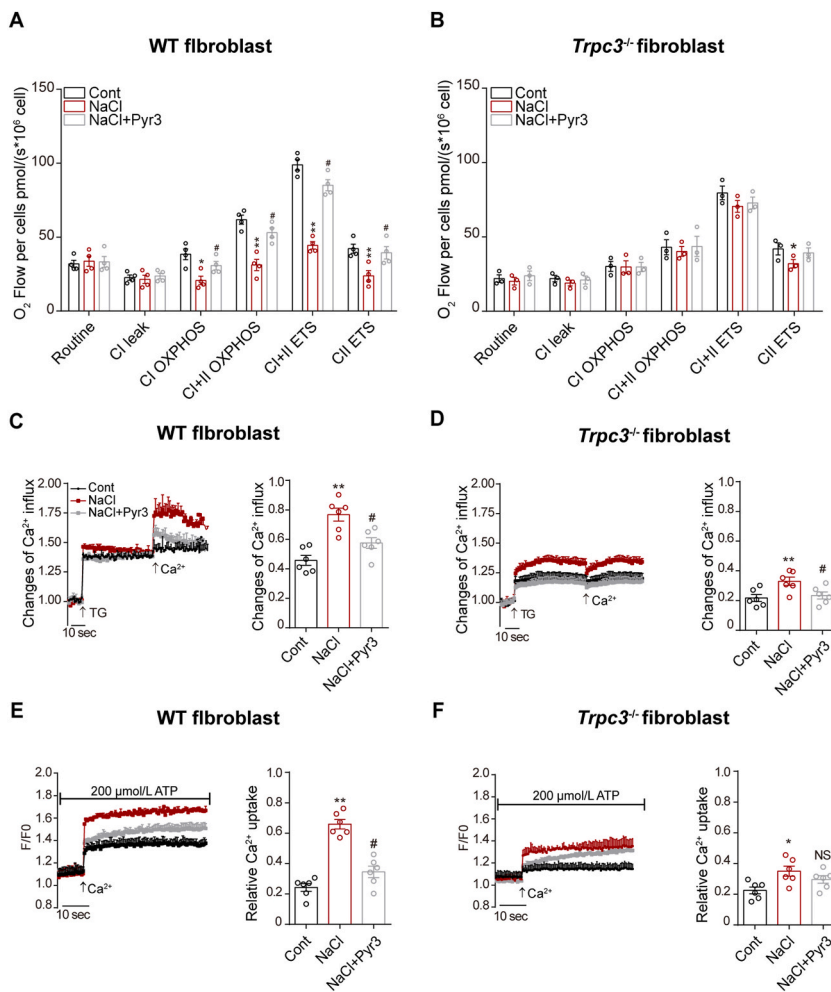

Fig. 4. TRPC3 deficiency improves high salt inhibition of mitochondrial respiratory function. Mitochondrial oxygen consumption was measured in dermal fibroblasts under control conditions (Cont) or under NaCl alone (20 mmol/L) or with NaCl (20 mmol/L) plus Pyr3 (10 μmol/L) for 24 h by Oxygraph-2k high-resolution respirometry. (**A and B**) Oxygen consumption capacity in dermal fibroblasts from WT mice or *Trpc3*$^{-/-}$ mice. n = 3. (**C and D**) Original fluorescence traces of thapsigargin (TG)-induced store-operated calcium influx in primary cultured fibroblasts from WT or *Trpc3*$^{-/-}$ mice. Summary data of changes in SOCE Ca^{2+} influx. (**E and F**) Original fluorescence traces of ATP-induced mitochondrial calcium uptake in primary cultured fibroblasts from WT or *Trpc3*$^{-/-}$ mice. *$P < 0.05$, **$P < 0.01$, Cont versus NaCl; #$P < 0.05$, NaCl versus NaCl + Pyr3; unpaired 2-tailed *t*-test. Data are the mean ± SEM. n = 6.

2.3. High salt activation of TRPC3 attenuates mitochondrial respiratory function and alters mitochondrial ultrastructure

Mitochondrial energy metabolism contributes significantly to the differentiation of cells. These related parameters were tested to determine how high salt affects mitochondrial respiratory function. The results showed that respiratory parameters of mitochondria, including CI OXPHOS, CI + II OXPHOS, CI + II ETS and CII ETS, were significantly decreased in dermal fibroblasts treated with high NaCl concentrations compared to the control group from WT mice. However, Pyr3 significantly reduced these effects of high NaCl in WT mice but not in $Trpc3^{-/-}$ mice (Fig. 4A–B, Supplemental Figs. 4A–4B). Moreover, high NaCl significantly elevated $[Ca^{2+}]_{cyt}$ and $[Ca^{2+}]_{mito}$ uptake, and TRPC3 inhibitor Pyr3 treatment significantly reduced these effects of high NaCl in WT but not in $Trpc3^{-/-}$ mice (Fig. 4C–F). Furthermore, high NaCl concentration treatment also significantly elevated ROS generation (Fig. 5A–F) and hydrogen peroxide (H_2O_2) production but reduced ATP production in primary cultured fibroblasts of WT mice. In contrast, Pyr3 significantly reduced the effects of high NaCl concentrations in WT but not $Trpc3^{-/-}$ mice (Supplemental Figs. 4A–5D). Specifically, high salt
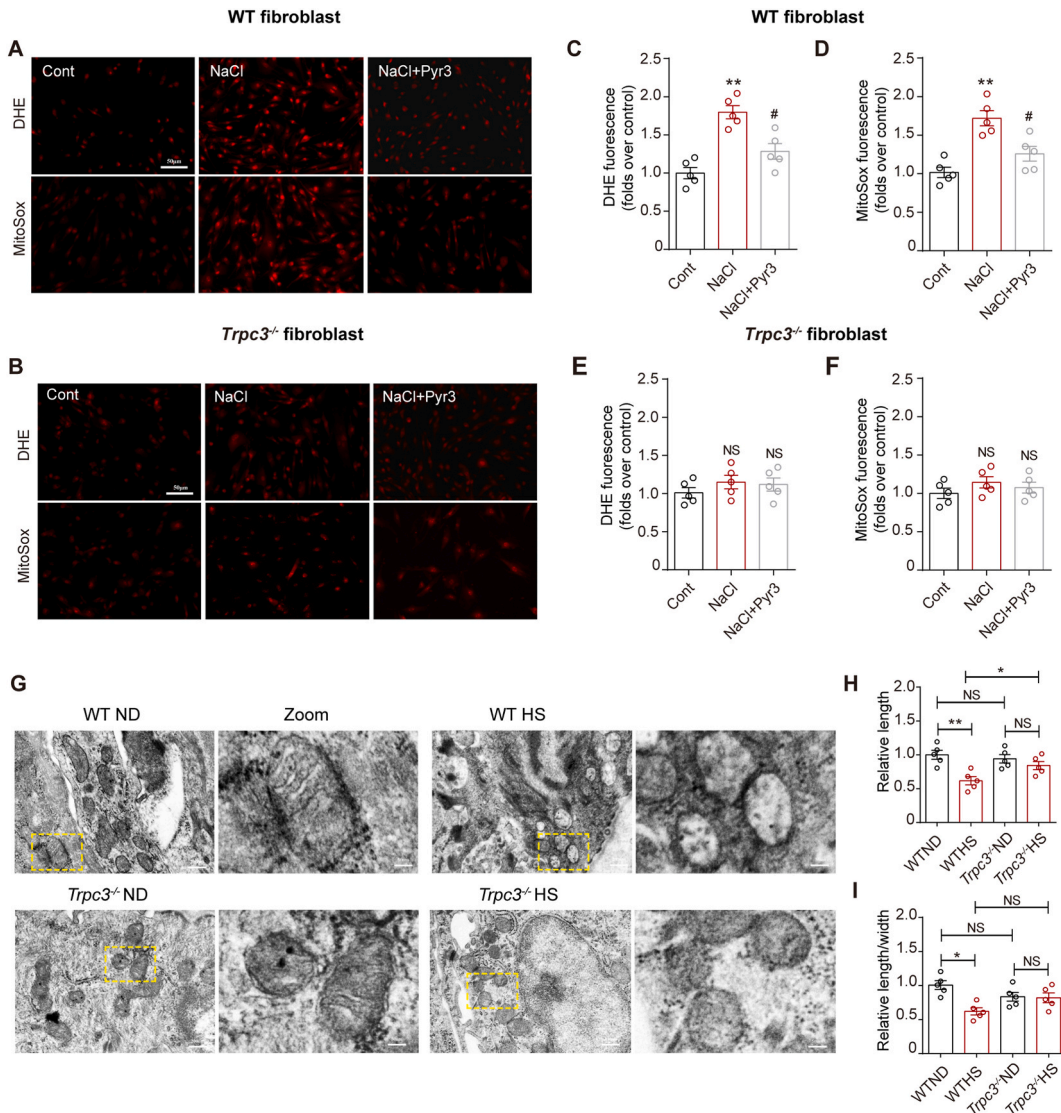

Fig. 5. High salt activation of TRPC3 elevates ROS production and alters the mitochondrial ultrastructure. (A and B) The effect of high NaCl (20 mmol/L) or Pyr3 (10 μmol/L) on cellular ROS levels by DHE staining or mitochondrial ROS levels by MitoSOX staining in wound tissue sections from WT and $Trpc3^{-/-}$ mice. Scale bar: 50 μm. (C–F) Summarized data of DHE and MitoSox staining in dermal fibroblasts of WT mice and $Trpc3^{-/-}$ mice. **$P < 0.01$, Cont versus NaCl; $^{\#}P < 0.05$, NaCl versus NaCl + Pyr3; n = 5. (G) Representative images of mitochondrial ultrastructure were analyzed by transmission electron microscopy (TEM) in skin tissues of WT mice and $Trpc3^{-/-}$ mice fed a ND or HS. Scale bar: 50 nm or 200 nm. Mitochondria are indicated by yellow arrows. (H and I) Quantitative data of mitochondrial relative length and ratio of length to width. *$P < 0.05$, **$P < 0.01$, ND versus HS; NS, NS, no significant difference. n = 5. Unpaired 2-tailed t-test. Data are the mean ± SEM. (For interpretation of the references to colour in this figure legend, the reader is referred to the Web version of this article.)

significantly upregulated the ratio of phosphorylated pyruvate dehydrogenase E1a subunit (phospho-PDHE1a) to total PDHE1a in WT but not $Trpc3^{-/-}$ mice. Meanwhile, $Trpc3^{-/-}$ significantly attenuated the effect of high NaCl (Supplemental Figs. 5E and 5F).

Mitochondrial ultrastructure is important for maintaining proper mitochondrial function. We further observed mitochondrial morphology in skin tissues by transmission electron microscopy (TEM). In skin tissues of WT mice fed an ND, mitochondria presented a bilayer membrane ultrastructure and wrinkled cristae, with the inner membrane folded into cristae. However, the skin tissues of WT mice fed an HS featured swollen mitochondria, cristae effacement and vacuolization. In addition, mitochondria exhibited a significant reduction in mitochondrial length and aspect ratio in WT mice fed an HS. These changes did not significantly differ in skin tissues from $Trpc3^{-/-}$ mice fed a ND or HS (Fig. 5G–I). Taken together, our data imply that a long-term high salt diet may impair mitochondrial respiratory function and alter mitochondrial ultrastructure during wound healing in a TRPC3-dependent manner.

2.4. High salt leads to delayed wound healing associated with decreased mitochondrial ATP metabolism in a TRPC3-dependent manner

We further investigated whether high salt affects wound healing. In vitro, analysis of collagen gel contraction showed that high salt enhanced fibroblast contraction in WT but not in $Trpc3^{-/-}$ mice. Pyr3 treatment inhibited the effect of high salt (Fig. 6A–C). In vivo, 2 full-thickness wounds on the back were applied to WT mice and $Trpc3^{-/-}$ mice (Fig. 6D). The results showed that WT mice fed an HS had a significantly slower wound healing rate in the early stage (0–3 days) and even in the later stage (3–9 days) than WT mice fed an ND. TRPC3 deficiency attenuated the high salt diet, leading to delayed wound healing (Fig. 6E–G).

Furthermore, chronic high salt treatment significantly increased actomyosin structure organization and response to metal ions but decreased mitochondrial respiratory chain complex I assembly and oxidative phosphorylation in wound granulation tissues from WT but not $Trpc3^{-/-}$ mice fed an HS (Fig. 7A–B, Supplemental Figs. 6C–6D). These data illustrate that a long-term high salt diet may impair
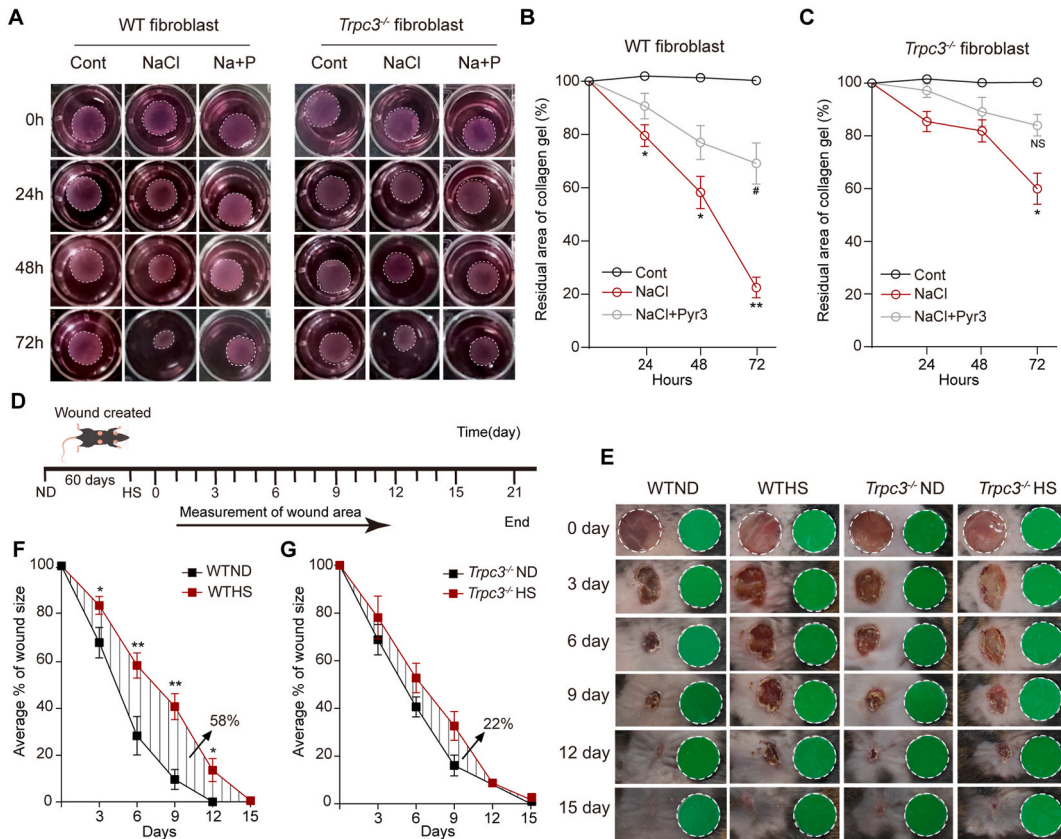

Fig. 6. Effect of high salt concentrations on dermal fibroblast contraction and impaired wound healing in vivo. (**A**) Effect of high salt concentrations on collagen gel contraction in dermal fibroblasts from WT mice or $Trpc3^{-/-}$ mice. Primary cultured dermal fibroblasts were treated with NaCl alone (20 mmol/L) or NaCl (20 mmol/L) plus Pyr3 (10 μmol/L) (Na + P) for 0 h, 24 h, 48 h and 72 h. (**B and C**) Summary data of cell contraction (residual area of collagen gel, %) in cultured dermal fibroblasts of WT and $Trpc3^{-/-}$ mice. *$P < 0.05$, Cont versus NaCl; #$P < 0.05$, NaCl versus NaCl + Pyr3; 2-way ANOVA followed by Bonferroni post hoc test. Data are the mean ± SEM, n = 3. (**D and E**) The cutaneous wounds were applied to the backs of mice after feeding on a ND or HS for 2 months, and the closure wounds were monitored at the desired times in this 15-day period after being fed a ND or HS. (**F and G**) The relative size of wounds is plotted, and AUC % of wound healed over time in WT or $Trpc3^{-/-}$ mice fed an ND or HS during wound healing. *$P < 0.05$, **$P < 0.01$, ND versus HS; 2-way ANOVA followed by Bonferroni post hoc test. Data are the mean ± SEM. A total of seven mice were tested independently three times, followed by pooling the wound counts from each group (n = 10–13).

mitochondrial ATP metabolism in a TRPC3-dependent manner.

2.5. TRPC3 deficiency attenuates the high salt elevation of hypertrophic scars through inhibition of the pMLC/pMYPT1 pathway

Differentially expressed genes were selected, and clustering analysis revealed that chronic high salt treatment significantly elevated myosin filament, myosin filament-based movement and actin-mediated cell contraction genes, such as Myh1, Myh6, Myh8, Myh9,
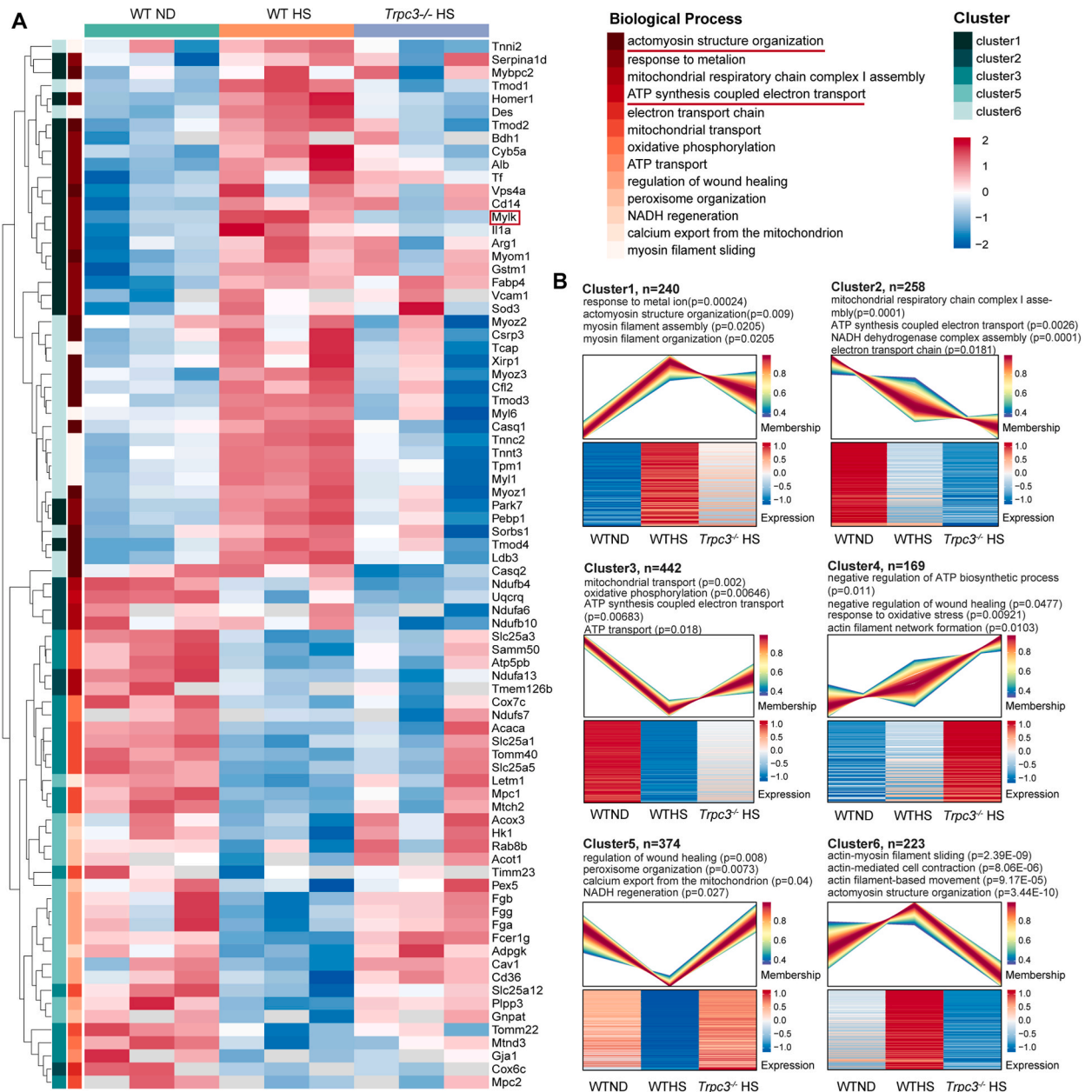

Fig. 7. TRPC3 deficiency reversed the high salt-elevated myosin filament and actin-mediated cell contraction genes but impaired mitochondrial ATP metabolism-related genes. (A) Heatmap representation of 2-fold changes or more genes of mitochondrial ATP metabolism-related and myosin-related biological processes in granulation tissues from WT mice fed a normal diet (0.25% NaCl, WT-ND), WT mice fed an 8% high-salt diet (WT-HS) or *Trpc3*−/− mice fed an HS (*Trpc3*-/HS) for 2 months. Then, the cutaneous wounds were applied to the backs of mice, and wound granulation tissues were analyzed after injury at 7 days. Each n = 3 (biological). **(B)** Differentially expressed genes were selected, and clustering analysis revealed that chronic high salt treatment significantly elevated myosin filament, myosin filament-based movement and actin-mediated cell contraction genes but decreased the regulation of wound healing in wound granulation tissues in WT mice fed HS but not *Trpc3*−/−− mice fed HS.

Myl1, Myl9, Mylpf and Mylk, but decreased the regulation of wound healing in wound granulation tissues in WT mice fed an HS but not *Trpc3*$^{-/-}$ mice (Supplemental Figs. 6A–6B). Chronic high salt provided significant elevation in protein expression of αSMA, TRPC3, fibronectin, collagen-1 (Col1a1), pMYPT/MYPT and pMLC/MLC in wound granulation tissues from WT mice fed an HS but not *Trpc3*$^{-/-}$ mice (Fig. 8A–C). Furthermore, hypertrophic scar skin tissues also demonstrated these protein expression changes compared with normal skin tissues in patient samples (Fig. 8D–F). In summary, these data indicate that chronic high-salt diets activate TRPC3-mediated Rho kinase pathways, promoting hypertrophic scar formation. TRPC3 deficiency may prevent hypertrophic scarring during wound healing.

3. Discussion

This study is the first to provide important evidence that high salt treatment enhances TRPC3 expression and function, which contributes to mitochondrial dysfunction and excessive ROS generation in dermal fibroblasts. High salt treatment increases myofibroblast differentiation and collagen deposition by activation of TRPC3-mediated pMLC/pMYPT1 pathway. TRPC3 deficiency attenuates high salt diet-induced hypertrophic scarring. The study highlights TRPC3 as a high salt sensitiveness controller of hypertrophic scar during wound healing.

TRP channels play key roles in proliferation, dermal fibrosis and wound healing [25,26]. TRP channel regulation of angiogenesis, nerve growth, cell proliferation and excessive collagen production associated with skin scarring. TRPV2 expressed within the epidermis and keratinocyte layers regulates intracellular Ca^{2+} homeostasis [27]. TRPV3 regulates dermal fibrosis in heat-induced oral epithelial proliferation and wound healing by decreasing ECM production [28]. Intracellular Ca^{2+} performs a major function in
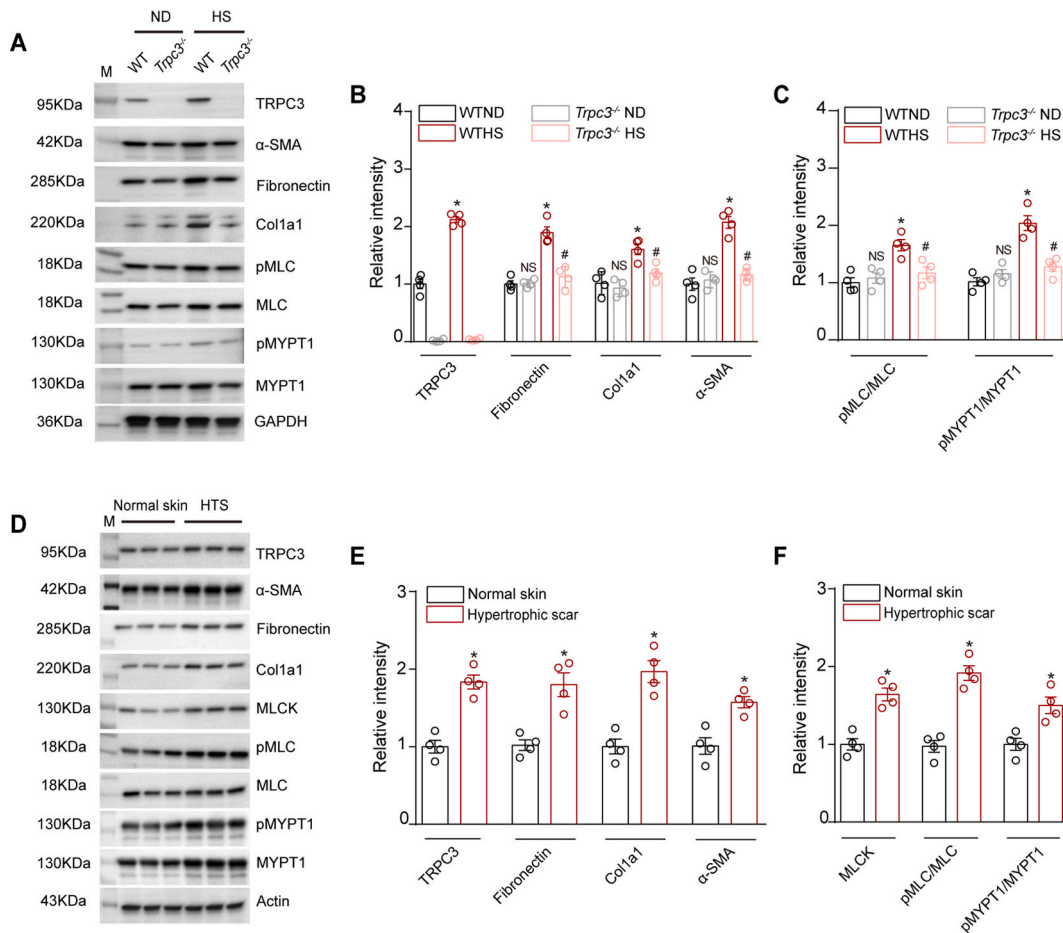

Fig. 8. TRPC3 deficiency attenuates high salt-induced myofibroblast transdifferentiation and hypertrophic scarring by inhibiting pMLC/pMYPT1. (**A**) Western blots and (**B and C**) quantitative analysis of α-SMA, TRPC3, Col1a1, fibronectin, pMYPT1 and pMLC in wound granulation tissues from WT mice or *Trpc3*$^{-/-}$ mice fed an ND or HS for 2 months. Then, the cutaneous wounds were applied to the backs of mice and wound granulation tissues. *$P < 0.05$, WT-ND versus WT-HS; #$P < 0.05$, WT-HS versus *Trpc3*$^{-/-}$ HS; NS, no significant difference. One-way ANOVA followed by Tukey's post hoc test. Data are the mean ± SEM, n = 4. (**D**) Western blots and (**E and F**) analysis of the protein expression of αSMA, TRPC3, Col1a1, fibronectin, pMYPT1 and pMLC in normal skin tissues and hypertrophic scars from patients. *$P < 0.05$. Unpaired 2-tailed *t*-test. Data are the mean ± SEM, n = 4.

controlling cell proliferation, differentiation and migration [29]. Calcium-binding proteins related to chronic inflammatory responses in keratinocytes of burn-wounded skin. Our previous study indicated that TRPC3 is involved in high salt-induced cardiac hypertrophy and high blood pressure [1]. However, it is not clear whether high salt levels regulate intracellular Ca^{2+} associated with myofibroblast differentiation and hypertrophic scarring during wound healing.

Skin scarring and fibrosis in injured tissue are related to endoplasmic reticulum Ca^{2+} store release, which disrupts intracellular Ca^{2+} homeostasis [30]. Our previous study demonstrated that elevated TGFβ1-induced store-operated Ca^{2+} entry was associated with myofibroblast differentiation in dermal fibroblasts [19]. In this study, we provide evidence to show that high salt activation of TRPC3 mediated mitochondrial Ca^{2+} overload by 1.75-fold, which promoted myofibroblast differentiation. Furthermore, long-term high salt intake elevated collagen deposition and delayed wounded healing in WT mice but not $Trpc3^{-/-}$ mice. Therefore, targeting TRPC3 may prevent high salt-mediated hypertrophic scarring during wound healing.

Mitochondrial oxidative respiration of keloid skin fibroblasts was impaired compared with that of normal skin fibroblasts. We provide evidence that high salt significantly increased the phosphorylation of PDHE1α by 90% compared to that in the control group, resulting in impaired mitochondrial respiratory function and promotion of ROS production in the electron transfer chain. TRPC3 deficiency significantly blunted the effect of high salt in dermal fibroblasts. Furthermore, another study showed that a high-salt diet for 15 days delayed wound healing by reducing noninflammatory innate immune cell activation [3]. Our study demonstrated that a chronic high-salt diet delayed wound healing related to TRPC3-mediated ROS activation of the RhoA/Rho kinase pathway.

Rho kinase (ROCK) and Rho A coordinate myosin II activity and promote actin filament aggregation to produce contractile forces [31], resulting in increased wound fibrosis [32]. Inhibition of Rho-associated signaling decreases collagen synthesis in cardiac fibroblasts and pulmonary fibrosis [33]. Furthermore, Rho-associated kinase inhibitors prevented excessive scarring by reducing wound contracture in rat models [34]. MLC and pMYPT1 are key mediators of cell proliferation in fibroblasts and keratinocytes [22,23]. In this study, long-term excessive salt consumption enhanced TRPC3-mediated excessive ROS generation, which activated MYPT1 phosphorylation at Ser695 in dermal fibroblasts. Long-term high salt diet attenuates mitochondria function and ultrastructural alterations involved in hypertrophic scar formation in a TRPC3-dependent manner. Inhibition of TRPC3-mediated Rho signaling may prevent hypertrophic scarring.

In summary, the study demonstrates a potential mechanism by which high salt activates TRPC3-mediated mitochondrial Ca^{2+} and excessive ROS generation in dermal fibroblasts. A chronic high-salt diet promotes dermal myofibroblast differentiation and hypertrophic scarring. TRPC3 acts as a salt-sensitive regulator to prevent hypertrophic scarring during wound healing.

4. Methods

4.1. Patients and ethics statement

Normal skin (NS, n = 6) and hypertrophic scar (HS, n = 6) tissues were collected from patients. Prior to surgery, participants were told about the objective and methods of the study and accepted to participate in this study. All participants who took part in the trial signed an informed agreement, and The Ethics Committee at Daping Hospital, Army Military Medical University, accepted the trial.

4.2. Animal care and open wound creation

Male TRPC3 knockout mice ($Trpc3^{-/-}$) and their wild-type littermates (WT) at the age of eight weeks were provided as a gift from Dr. Birnbaumer (Laboratory of Neurobiology, National Institute of Environmental Health Sciences, National Institutes of Health, Research Triangle Park, USA). According to our previous publication, homozygotes, heterozygotes, and WT littermates were recognized [19]. The animals were kept in a regulated temperature (21°C–23 °C) environment with a 12/12-h light-dark cycle and unrestricted access to food and water. Briefly, $Trpc3^{-/-}$ mice (n = 12) and WT mice (n = 12) were divided into randomized groups and given either a normal diet (ND, 0.25% NaCl) or a high salt concentration diet (HS, 8% NaCl) for 60 days. Then, on the back skin of the mice, open incisions were made. The mice were under anesthesia with 2.5% sevoflurane and kept with 2% sevoflurane. (Matrx VIP 3000, Isoflurane Vaporizer). The back hair of the mice was neatly removed and sanitized with Iodophor. The dorsal area was disinfected with iodophor and 75% ethanol, and each mouse was subjected to two 8-mm circular excision wounds made with scissors above the fascia layer. The postoperative diets of the mice were maintained on an HS as the experimental group and an ND as the control group. Wound area measurements were performed at 0, 3, 6, 9, 12, and 15 days after injury, and samples were obtained at 7, 14 and 21 days after injury. The wound healing rate was determined utilizing ImageJ software (NIH). W_0 was defined as the initial area of the wound, and W_t was defined as the residual wound area. The wound healing rate was measured as follows: W% (% of wound size) = $W_t/W_0 \times 100\%$. All animal research was authorized by the Animal Ethics Committee of the Third Military Medical University.

4.3. Cell culture

Primary dermal fibroblasts were collected from the skin of 1- to 2-day-old $Trpc3^{-/-}$ and WT mice and grown in DMEM with low glucose (Gibco) culture media supplemented with 10% FBS (Corning) and 1% streptomycin/penicillin. Briefly, the epidermis was enzymatically digested with 0.25% Dispase II (Roche) and physically separated from the dermis using tweezers, and the dermal layers were sliced into small pieces and placed in digesting medium (5 mL DMEM supplemented with 10% FBS and 0.2% collagenase II, Diamond) in a rotating hybridization room at 37 °C for 8 h. Filtrated single-cell suspensions were created by spinning them down for 5 min at 500 rcf, followed by two PBS washes. Every three days, the cells were passaged, and 3.75×10^5 cells were injected into each 25

cm^2 culture container.

4.4. Immunohistochemistry and immunofluorescence staining

Briefly, $Trpc3^{-/-}$ mice (n = 6) and WT mice (n = 6) were randomly assigned to two groups and fed either a 0.25% NaCl diet or an 8% NaCl diet for eight weeks. Afterward, two 8-mm full-thickness incisions were made on the backs of the mice, and wound skin samples were taken at 7, 14 and 21 days after injury. Fixation of all specimens was conducted with 4% paraformaldehyde, followed by dehydration, paraffin embedding, and sectioning into 5 μm sections. Immunohistochemistry or immunofluorescence staining was performed. The primary antibodies applied were anti-αSMA (1:150, Abcam, ab7817), anti-TRPC3 (1:200, Alomone, ACC-016), anti-CD31 (1:100, Abcam, ab222783) and anti-vimentin (1:200, Abcam, ab8978), and the secondary antibody with fluorescent label was purchased from Beyotime (China). Microscopy (D80, Nikon) was used to examine and photograph all sections. Confocal images were captured using an A1R + Nikon confocal microscope and quantified by ImageJ software (NIH). The results were then presented as the mean optical density and were normalized to control group. Mean optical density = integrated optical density/area (mm^2). The vascular objects ($CD31^+$) were counted to determine vascular density (vessel/mm^2). A random sample of five high-power field views was chosen from each slice for calculation and statistical analysis.

4.5. Western blot

Western blot assays were performed as described earlier [19]. A buffer was used to lyse cells or tissues, followed by 20 min of freezing at -20 °C. Insoluble debris from the sample was removed by centrifuging it at $12000 \times g$ at 4 °C for 20 min. Next, the supernatant samples were collected, and protein levels were calculated by the Bradford method (Bio-Rad Protein Assay). The gray value of Western blot was quantified and normalized to the internal reference (GAPDH or Actin) with ImageJ software (NIH). We utilized the following primary antibodies: anti-α-smooth muscle actin (1:1000, ab7817); anti-TRPC3 (1:1000, Alomone, ACC-016); anti-collagen I (1:1000, Cell Signaling Technology, #84336); anti-MLC (1:1000, Cell Signaling Technology, #3675); anti-pMLC (1:1000, Cell Signaling Technology, #3672); anti-MYPT1 (1:1000, Santa Cruz Biotechnology, Sc-51426); anti-pMYPT1 (Santa Cruz Biotechnology, Sc-33360); anti-Fibronectin (1:1000, Abcam, ab268020); anti-phosphorylated Ser695 pyruvate dehydrogenase E1a subunit (PDHE1a) anti-pPDHE1a (1:1000, Merck-Millipore) and anti-GAPDH from Santa Cruz Biotechnology.

4.6. Transmission electron microscopy (TEM)

TEM was performed in the Third Military Medical University. The wound edge was dissected and cut into small pieces, approximately 1 mm^3 in volume. Tissue pieces were fixed in 2.5% glutaraldehyde for 1.5 h at 4 °C, postfixed 1% osmium tetroxide for 2 h, dehydrated in a graded ethanol series and then embedded in epoxy resin. Ultrathin sections (80 nm) were cut using an ultramicrotome with a diamond knife (Leica). TEM images were obtained on JEM-1400plus TEM (JEOL). Mitochondrial length and width were quantified using ImageJ (NIH).

4.7. High-resolution mitochondrial respiratory

Mitochondrial respiratory function was investigated by a fluorospectrometer with two channels for titration injection respirometers (Oxygraph-2k; Oroboros Instruments). The fibroblasts were pretreated with NaCl (20 mmol/L) or NaCl plus Pyr3 (10 μmol/L) for 24 h, while an equivalent amount of PBS was added to the control group. Trypsin digestion was used to extract fibroblasts, which were then centrifuged for 6 min at room temperature at 600 rpm. The fibroblast suspension was injected separately into the oxygraph chambers at a density of $\approx 2*10^6$ cells/mL. After equalizing respiration, routine respiration (without additives) was measured. Then, a titration of digitonin (100μg/10^6 cells) was applied to cause permeabilization of the plasma membrane. When glutamate (5 mmol/L) and malate (2 mmol/L) were titrated without ADP, the respiratory leak state of complex I (CI leak) was identified. After adding 5 mmol/L ADP, the oxidative phosphorylation capacity of CI was exhibited (CI OXPHOS). The addition of succinate (100 mmol/L) triggered the oxidative phosphorylation function of CI and CII (CI + CII OXPHOS). Afterward, carbonyl cyanide 4-trifluoromethoxy phenylhydrazone (FCCP) injection up to 1.5 μmol/L was instantly titrated to attain the maximum uncoupled respiratory capacity of the electron transfer system (CI + CII ETS). After adding rotenone (0.5 mol/L), the uncoupled respiratory capacity of CII (CII ETS) was analyzed.

4.8. Measurement of ROS levels

The cytosolic ROS levels were determined by the fluorescent probe dihydroethidium (DHE, Thermo Fisher Scientific), and mitochondrial ROS levels were assessed with MitoSOX Red (Thermo Fisher Scientific). Concentrations of ROS were normalized based on the fluorescence intensity of control cells. The glass slides were viewed under an inverted fluorescence microscope (TE2000; Nikon) equipped with a PlanFluor objective lens of 10X. Using NIS-Elements 3.0 software (Nikon Instruments), photographs were obtained, and the fluorescence intensity was assessed.

4.9. Intracellular and mitochondrial Ca^{2+} measurement

Fura-2AM and Rhod-2AM (Thermo Fisher Scientific) were utilized to determine the concentrations of cytosolic Ca^{2+} ($[Ca^{2+}]_{cyt}$) and mitochondrial Ca^{2+} ($[Ca^{2+}]_{mito}$) as previously described [19]. Briefly, for $[Ca^{2+}]_{cyt}$, a 30-min dark incubation with Fura-2 AM and F-127 was performed on cells. Afterward, the cells were resuspended in Ca^{2+}-free Hank's balanced salt solution (HBSS) after three washings. The fluorescence intensity was determined at 510 nm for emission and 340 and 380 nm for excitation. For $[Ca^{2+}]_{mito}$, cells were incubated with Rhod-2 AM (5 μmol/L) and F-127 (0.025%) for half an hour in the dark at 37 °C. Afterward, an extracellular solution was used three times to wash them. The fluorescent intensity was measured at an emission wavelength of 581 nm and excitation wavelength of 552 nm.

4.10. Cell contraction test

A solution of NaOH (0.1 mol/L) was employed to modify the pH of commercial rat tail type I collagen (Solarbio, China) to neutral. Fibroblasts (1×10^5) were treated with NaCl (20 mmol/L), NaCl plus Pyr3 (10 μmol/L) or without NaCl as a control group for 24, 48 and 72 h. Then, harvested fibroblasts were resuspended in culture medium with a mixed pH neutral rat tail collagen solution containing 1 mg/mL collagen. Each well of 24-well plates was filled with 1 mL of rat tail collagen solution containing fibroblasts, and the plates were kept at room temperature for 20 min to enable coagulation of the solution into a gel. Each group of plates was cultured at 37 °C in a 5% CO_2 incubator after adding appropriate volumes of culture medium and stimulants. Every 12 h, images were taken, and collagen gel areas were measured using ImageJ software (NIH).

4.11. RT–PCR

Total RNA was isolated from fibroblasts using TRIzol (Invitrogen, Carlsbad, CA). First strand cDNA was synthesized using Evoscript Universal cDNA Master Mix. PCRs were performed according to the instructions of the manufacturer (Light Cycler 96, Roche) using the QuantiTect SYBR Green RT–PCR Kit (QIAGEN). Using the second derivative method, crossing points were determined with Light Cycler analysis software (Life Technologies, Norwalk, CT). Normalized data were collected using housekeeping genes (GAPDH). The primer sequences for the target gene α-SMA were CCC AGA CAT CAG GGA GTA ATG G (forward) and TCT ATC GGA TAC TTC AGC GTC A (reverse). For TRPC3: CAA GAA TGA CTA TCG GAA GC (forward) and GCC ACA AAC TTT TTG ACT TC (reverse). For GAPDH, the primers were AAC TGC TTA GCA CCC CTG GC (forward) and ATG ACC TTG CCC ACA GCC TT (reverse).

4.12. Statistical analysis

All findings are displayed as the mean ± SEM. Statistical analysis was performed by GraphPad Prism 8.0 (GraphPad Software) or SPSS 17.0. A Kolmogorov–Smirnov test was applied to assess the data normality, and Student's t tests or Mann–Whitney U tests were employed, depending on whether the data were parametric or nonparametric. For analysis of more than 2 groups, 1-way or 2-way ANOVA was performed, and for all significant outcomes, Tukey's or Bonferroni's post hoc comparison was performed. A value of $P < 0.05$ was considered statistically significant.

5. Study approval

Animal research was carried out according to protocols authorized by the Army Medical University's Animal Ethics Committee. Patients submitted written informed permission for human trials, and the protocol was approved by local ethics committees.

Author contribution statement

Weijie Xia: Conceived and designed the experiments; Performed the experiments; Analyzed and interpreted the data; Wrote the paper.

Qianran Wang: Performed the experiments; Analyzed and interpreted the data; Wrote the paper.

Shaoyang Lin, Yuanyuan Wang, Junbo Zhang, Hailin Wang, Xia Yang, Yingru Hu: Performed the experiments.;

Huaping Liang, Yuangang Lu: Contributed reagents, materials, analysis tools or data.

Zhiming Zhu: Contributed reagents, materials, analysis tools or data; Wrote the paper.

Daoyan Liu: Conceived and designed the experiments; Analyzed and interpreted the data; Wrote the paper.

Data availability statement

The data that has been used is confidential.

Declaration of competing interest

The authors declare the following financial interests/personal relationships which may be considered as potential competing interests: Daoyan Liu reports financial support was provided by National Natural Science Foundation of China.

Acknowledgments

Appendix A. Supplementary data

Supplementary data to this article can be found online at https://doi.org/10.1016/j.heliyon.2023.e18629.

References

[1] T. Ma, S. Lin, B. Wang, Q. Wang, W. Xia, H. Zhang, et al., TRPC3 deficiency attenuates high salt-induced cardiac hypertrophy by alleviating cardiac mitochondrial dysfunction, Biochem. Biophys. Res. Commun. 519 (4) (2019) 674–681.

[2] B. Sundstrom, I. Johansson, S. Rantapaa-Dahlqvist, Interaction between dietary sodium and smoking increases the risk for rheumatoid arthritis: results from a nested case-control study, Rheumatology 54 (3) (2015) 487–493.

[3] K.J. Binger, M. Gebhardt, M. Heinig, C. Rintisch, A. Schroeder, W. Neuhofer, et al., High salt reduces the activation of IL-4- and IL-13-stimulated macrophages, J. Clin. Invest. 125 (11) (2015) 4223–4238.

[4] M.E. Marketou, S. Maragkoudakis, I. Anastasiou, H. Nakou, M. Plataki, P.E. Vardas, et al., Salt-induced effects on microvascular function: a critical factor in hypertension mediated organ damage, J. Clin. Hypertens. 21 (6) (2019) 749–757.

[5] A. Dahlmann, K. Dorfelt, F. Eicher, P. Linz, C. Kopp, I. Mossinger, et al., Magnetic resonance-determined sodium removal from tissue stores in hemodialysis patients, Kidney Int. 87 (2) (2015) 434–441.

[6] H. Wiig, A. Schroder, W. Neuhofer, J. Jantsch, C. Kopp, T.V. Karlsen, et al., Immune cells control skin lymphatic electrolyte homeostasis and blood pressure, J. Clin. Invest. 123 (7) (2013) 2803–2815.

[7] X.Z. Bai, J.Q. Liu, L.L. Yang, L. Fan, T. He, L.L. Su, et al., Identification of sirtuin 1 as a promising therapeutic target for hypertrophic scars, Br. J. Pharmacol. 173 (10) (2016) 1589–1601.

[8] S. Jimi, M. Kimura, F. De Francesco, M. Riccio, S. Hara, H. Ohjimi, Acceleration mechanisms of skin wound healing by autologous micrograft in mice, Int. J. Mol. Sci. 18 (8) (2017).

[9] G.G. Gauglitz, H.C. Korting, T. Pavicic, T. Ruzicka, M.G. Jeschke, Hypertrophic scarring and keloids: pathomechanisms and current and emerging treatment strategies, Mol. Med. 17 (1–2) (2011) 113–125.

[10] C.C. Finnerty, M.G. Jeschke, L.K. Branski, J.P. Barret, P. Dziewulski, D.N. Herndon, Hypertrophic scarring: the greatest unmet challenge after burn injury, Lancet 388 (10052) (2016) 1427–1436.

[11] P. Ahangar, X.L. Strudwick, A.J. Cowin, Wound healing from an actin cytoskeletal perspective, Cold Spring Harbor Perspect. Biol. 14 (8) (2022).

[12] J. Janossy, P. Ubezio, A. Apati, M. Magocsi, P. Tompa, P. Friedrich, Calpain as a multi-site regulator of cell cycle, Biochem. Pharmacol. 67 (8) (2004) 1513–1521.

[13] K.M. McAndrews, T. Miyake, E.A. Ehsanipour, P.J. Kelly, L.M. Becker, D.J. McGrail, et al., Dermal alphaSMA(+) myofibroblasts orchestrate skin wound repair via beta1 integrin and independent of type I collagen production, EMBO J. 41 (7) (2022), e109470.

[14] L. Petecchia, F. Sabatini, C. Usai, S. Carnevali, M. Ognibene, C. Vanni, et al., Mechanisms of bradykinin-induced contraction in human fetal lung fibroblasts, Eur. Respir. J. 36 (3) (2010) 655–664.

[15] B. Wang, S. Xiong, S. Lin, W. Xia, Q. Li, Z. Zhao, et al., Enhanced mitochondrial transient receptor potential channel, canonical type 3-mediated calcium handling in the vasculature from hypertensive rats, J. Am. Heart Assoc. 6 (7) (2017).

[16] J.D. Rhodes, J. Sanderson, The mechanisms of calcium homeostasis and signalling in the lens, Exp. Eye Res. 88 (2) (2009) 226–234.

[17] Z. Xu, C. Cheng, R. Kong, Y. Liu, S. Wang, Y. Ma, et al., S100A8 and S100A9, both transcriptionally regulated by PU.1, promote epithelial-mesenchymal transformation (EMT) and invasive growth of dermal keratinocytes during scar formation post burn, Aging (Albany NY) 13 (11) (2021) 15523–15537.

[18] F. Lu, J. Gao, R. Ogawa, C. Hyakusoku, C. Ou, Fas-mediated apoptotic signal transduction in keloid and hypertrophic scar, Plast. Reconstr. Surg. 119 (6) (2007) 1714–1721.

[19] W. Xia, Q. Wang, Y. Lu, Y. Hu, X. Zhang, J. Zhang, et al., Transient receptor potential channel canonical type 3 deficiency antagonizes myofibroblast transdifferentiation in vivo, BioMed Res. Int. 2020 (2020), 1202189.

[20] E. Bertero, C. Maack, Calcium signaling and reactive oxygen species in mitochondria, Circ. Res. 122 (10) (2018) 1460–1478.

[21] D.B. Zorov, M. Juhaszova, S.J. Sollott, Mitochondrial reactive oxygen species (ROS) and ROS-induced ROS release, Physiol. Rev. 94 (3) (2014) 909–950.

[22] S. Hiroyasu, G.P. Stimac, S.B. Hopkinson, J.C.R. Jones, Loss of beta-PIX inhibits focal adhesion disassembly and promotes keratinocyte motility via myosin light chain activation, J. Cell Sci. 130 (14) (2017) 2329–2343.

[23] D.H. Freed, L. Chilton, Y. Li, A.L. Dangerfield, J.E. Raizman, S.G. Rattan, et al., Role of myosin light chain kinase in cardiotrophin-1-induced cardiac myofibroblast cell migration, Am. J. Physiol. Heart Circ. Physiol. 301 (2) (2011) H514–H522.

[24] J.H. Brown, D.P. Del Re, M.A. Sussman, The Rac and Rho hall of fame: a decade of hypertrophic signaling hits, Circ. Res. 98 (6) (2006) 730–742.

[25] M.M. Moran, TRP channels as potential drug targets, Annu. Rev. Pharmacol. Toxicol. 58 (2018) 309–330.

[26] Y. Okada, T. Sumioka, P.S. Reinach, M. Miyajima, S. Saika, Roles of epithelial and mesenchymal TRP channels in mediating inflammatory fibrosis, Front. Immunol. 12 (2021), 731674.

[27] T. Ishii, K. Uchida, S. Hata, M. Hatta, T. Kita, Y. Miyake, et al., TRPV2 channel inhibitors attenuate fibroblast differentiation and contraction mediated by keratinocyte-derived TGF-beta1 in an in vitro wound healing model of rats, J. Dermatol. Sci. 90 (3) (2018) 332–342.

[28] J.Y. Um, S.Y. Kang, H.J. Kim, B.Y. Chung, C.W. Park, H.O. Kim, Transient receptor potential vanilloid-3 (TRPV3) channel induces dermal fibrosis via the TRPV3/TSLP/Smad2/3 pathways in dermal fibroblasts, J. Dermatol. Sci. 97 (2) (2020) 117–124.

[29] I.A. Darby, N. Zakuan, F. Billet, A. Desmouliere, The myofibroblast, a key cell in normal and pathological tissue repair, Cell. Mol. Life Sci. 73 (6) (2016) 1145–1157.

[30] B. Wang, A. Wen, C. Feng, L. Niu, X. Xiao, L. Luo, et al., The in vivo anti-fibrotic function of calcium sensitive receptor (CaSR) modulating poly(p-dioxanone-co-l-phenylalanine) prodrug, Acta Biomater. 73 (2018) 180–189.

[31] M. Amano, M. Ito, K. Kimura, Y. Fukata, K. Chihara, T. Nakano, et al., Phosphorylation and activation of myosin by Rho-associated kinase (Rho-kinase), J. Biol. Chem. 271 (34) (1996) 20246–20249.

[32] N. Watanabe, T. Kato, A. Fujita, T. Ishizaki, S. Narumiya, Cooperation between mDia1 and ROCK in Rho-induced actin reorganization, Nat. Cell Biol. 1 (3) (1999) 136–143.

[33] H. Zhou, K.X. Zhang, Y.J. Li, B.Y. Guo, M. Wang, M. Wang, Fasudil hydrochloride hydrate, a Rho-kinase inhibitor, suppresses high glucose-induced proliferation and collagen synthesis in rat cardiac fibroblasts, Clin. Exp. Pharmacol. Physiol. 38 (6) (2011) 387–394.

[34] J.E. Bond, G. Kokosis, L. Ren, M.A. Selim, A. Bergeron, H. Levinson, Wound contraction is attenuated by fasudil inhibition of Rho-associated kinase, Plast. Reconstr. Surg. 128 (5) (2011), 438e-50e.

[35] E.W. Deutsch, N. Bandeira, Y. Perez-Riverol, V. Sharma, J.J. Carver, L. Mendoza, et al., The ProteomeXchange consortium at 10 years: 2023 update, Nucleic Acids Res. 51 (D1) (2023) D1539–D1548.